Relativistic spin flip effect in attoclock

I. A. Ivanov,* A. S. Kheifets,† and A. S. Landsman[2‡]

Research School of Physics, Australian National University, Canberra ACT 2601, Australia

(Dated: May 15, 2025)

We study the effect of spin flip on tunneling ionization in the attoclock settings. Our study is based on a fully relativistic approach in which we seek a numerical solution of the time dependent Dirac equation (TDDE). We find that spin flip during strong field ionization significantly increases the attoclock offset angle, indicating longer tunneling delay relative to electrons with no spin flip. To interpret our numerical findings, we conduct additional modeling within the perturbative Breit-Pauli approach, which allows us to elucidate the role of different relativistic mechanisms. We show that the spin-orbit interaction is mainly responsible for the spin flip, rather than interaction with the magnetic component of the laser field. We further discuss the dynamic mechanisms of the spin flip effect, suggesting that it takes place while the electron is still bound. Our findings indicate that the attoclock can be used to investigate electron spin flip dynamics during the tunnel ionization process.

I. INTRODUCTION

It has long been recognized that relativistic effects such as electron spin reversal (spin-flip or SF) can occur in atomic or molecular photoionization for moderate laser fields intensities [1]. In the following years, the electron SF dynamics have been studied on the attosecond time scale in the context of single photon absorption [2–4]. In this case, spin-orbit (SO) effects can manifest themselves in the Wigner time delay of atomic photoemission, which can be extracted using linear streaking [5–9]. The SF process is explicitly recognized in these studies [4, 7, 9].

On the other hand, spin-flip dynamics during the strong field ionization is less understood

*Electronic address: Igor.Ivanov@anu.edu.au

†Electronic address: A.Kheifets@anu.edu.au

‡Electronic address: landsman.7@osu.edu

theoretically, and has not been investigated experimentally, although SF effects are believed to be an important part of the tunneling dynamics [19]. Attosecond angular streaking, known as attoclock, allows to resolve the dynamics of strong field tunnel ionization on the attosecond time scale [10, 11]. While the interpretation of the attoclock measurements of tunneling time is still a topic of debate [12–15], the attoclock remains the main tool for time-resolving attosecond dynamics of tunneling electrons [16, 17]. More recently, the attoclock has been used to investigate K-shell photoemission delays in ionization of molecules with attosecond X-ray pulses produced at the X-ray Free Electron Laser (XFEL) at LCLS [18].

Here, we propose to investigate the impact of the electron SF on the attoclock offset angle. By comparing this offset angle to that of electrons which do not undergo a SF, one can extract an additional delay associated with the SF process. To this end, we consider the process of tunneling ionization of the hydrogen and heavier atoms driven by circularly polarized laser pulses in the intensity range of 10^{14} W/cm^2. We model this process by solving the time-dependent Dirac equation (TDDE). We focus our attention on the photoelectron momentum distribution (PMD) in the plane of laser polarization. We derive radially integrated PMD and determine its angular offset relative to the electric field direction at the instant of tunneling. In the spirit of attoclock, such an offset is related with the tunneling time. We demonstrate that said angular offset is significantly affected by the SF process. By conducting further perturbative Breit-Pauli simulations, we disentangle various relativistic SF channels and attribute the observed effect to the SO coupling. In the meantime, the magnetic component of the laser field plays a negligible role in the SF process.

The rest of the paper is organized as follows. in Sec. II we outline our TDDE formalism II A and perturbative Breit-Pauli approach II B. Our main results are summarized and discussed in Sec. III. Conclusions are drawn and further directions are outlined in Sec. IV.

Atomic units with $\hbar = 1$, $e = 1$, $m = 1$, and $c \approx 137$ (here e and m are charge and mass of the electron, c- speed of light) are used throughout the paper.

II. THEORY

A. Time-dependent Dirac framework

We seek the solution of the TDDE using the procedure described in earlier works [20, 21]. For convenience, we recapitulate below the main features of the procedure, emphasizing the differences of the present calculation using a circularly polarized (CP) laser pulse and the work [21] where a linearly polarized driving laser pulse was considered.

We solve the TDDE for an atom in the field of a laser pulse

$$i\frac{\partial\Psi(\boldsymbol{r},t)}{\partial t} = \hat{H}\Psi(\boldsymbol{r},t)\ , \tag{1}$$

where $\Psi(\boldsymbol{r},t)$ is a four-component Dirac bispinor, $\hat{H}$ is the Hamiltonian operator:

$$\hat{H} = \hat{H}_{\rm atom} + \hat{H}_{\rm int} \tag{2}$$

with

$$\hat{H}_{\rm atom} = c\boldsymbol{\alpha}\cdot\hat{\boldsymbol{p}} + c^2(\beta - I) + IV(r) \tag{3}$$

and

$$\hat{H}_{\rm int} = c\boldsymbol{\alpha}\cdot\boldsymbol{A} \tag{4}$$

In Eq. (3) $\boldsymbol{\alpha} = \begin{pmatrix} \mathbf{0} & \boldsymbol{\sigma} \\ \boldsymbol{\sigma} & \mathbf{0} \end{pmatrix}$, $\beta = \begin{pmatrix} \boldsymbol{I} & \mathbf{0} \\ \mathbf{0} & -\boldsymbol{I} \end{pmatrix}$, $I = \begin{pmatrix} \boldsymbol{I} & \mathbf{0} \\ \mathbf{0} & \boldsymbol{I} \end{pmatrix}$, $\boldsymbol{\sigma}$ are Pauli matrices, $\mathbf{0}$ and $\boldsymbol{I}$ are 2×2 null and identity matrices, and c is the speed of light. We subtract from the field-free atomic Hamiltonian (3) the constant term Ic^2 corresponding to the rest mass energy of the electron to make the correspondence with the non-relativistic picture more transparent. The atomic potential $V(r)$ in Eq. (3) describes the target atom in the single active electron (SAE) approximation. We will be considering several targets below, with the SAE potentials given in [22].

We use the standard attoclock geometry with a CP laser pulse. The laser pulse propagates in the $x-$ direction. The vector potential in Eq. (4) is, therefore, of the form

$$\boldsymbol{A}(\boldsymbol{r},t) = \hat{\boldsymbol{y}}h_y(\zeta) + \hat{\boldsymbol{z}}h_z(\zeta)\ , \tag{5}$$

where $\zeta = t - \dfrac{x}{c}$, and $\hat{\boldsymbol{y}}$ and $\hat{\boldsymbol{z}}$ are the unit vectors along the $y-$ and $z-$ axes, respectively. The functions $h_y(\zeta)$ and $h_z(\zeta)$ have compact support, they are zero outside the interval

$(0, T)$. The parameter T has a meaning of the total pulse duration, as measured at any given spatial point.

Within the interval $(0, T)$ the functions $h_y(\zeta)$ and $h_z(\zeta)$ are given by the expressions

$$\begin{aligned} h_y(\zeta) &= \frac{E_0}{\omega\sqrt{2}} \sin^2\left(\frac{\Omega\zeta}{2}\right) \sin(\omega\zeta) \\ h_z(\zeta) &= \frac{E_0}{\omega\sqrt{2}} \sin^2\left(\frac{\Omega\zeta}{2}\right) \cos(\omega\zeta) \ , \end{aligned}$$

where $\Omega = 2\pi/T$, and E_0 is the peak electric field strength of the pulse. We will use below ultra-short pulses with the total duration of one optical cycle (o.c.) $T = 2\pi/\omega$ corresponding to the base laser frequency ω. With this choice $\Omega = \omega$ in Eq. (6). All the calculations performed below used the base frequency $\omega = 0.057$ a.u. (wavelength of 800 nm).

To solve the TDDE numerically we represent the solution as a series in basis bispinors:

$$\Psi(\boldsymbol{r}, t) = \sum_{\substack{j \\ l=j\pm 1/2}}^{J_{\max}} \sum_{M=-j}^{j} \Psi_{jlM}(\boldsymbol{r}, t) \ , \tag{6}$$

where

$$\Psi_{jlM}(\boldsymbol{r}, t) = \begin{pmatrix} g_{jlM}(r, t)\Omega_{jlM}(\boldsymbol{n}) \\ f_{jlM}(r, t)\Omega_{jl'M}(\boldsymbol{n}) \end{pmatrix} \ , \tag{7}$$

and the two-component spherical spinors are defined as

$$\Omega_{jlM}(\boldsymbol{n}) = \begin{pmatrix} C^{jM}_{l\ M-\frac{1}{2}\frac{1}{2}\frac{1}{2}} Y_{l,M-\frac{1}{2}}(\boldsymbol{n}) \\ C^{jM}_{l\ M+\frac{1}{2}\frac{1}{2}-\frac{1}{2}} Y_{l,M+\frac{1}{2}}(\boldsymbol{n}) \end{pmatrix} \ .$$

Here $C^{jM}_{lm\frac{1}{2}\mu}$ are the Clebsch-Gordan coefficients, $Y_{lm}(\boldsymbol{n})$ are the spherical harmonics and $\boldsymbol{n} = \boldsymbol{r}/r$. The angular momenta l and l' in Eq. (6) must satisfy the triangle relation $l + l' = 2j$.

To account for the non-dipole effects due to the spatial dependence of the laser field, the vector potential (5) is expanded in a series of spherical harmonics at every step of the integration procedure.

Spatial variables in the differential equations for the radial functions $g_{jlM}(r, t)$ and $f_{jlM}(r, t)$ were discretized on a grid with the step size $\delta r = 0.05$ a.u. The radial variable was restricted to an interval $(0, R_{\max})$, with $R_{\max} = 200$ a.u. The maximum value of the total momentum j in Eq. (6) was $J_{\max} = 40$ which, for the presently considered field

intensities in the range of 10^{14} W/cm^2 is sufficient to achieve convergence of the expansion (6).

The chosen computational strategy [20, 21] results in a set of the coupled differential equations for the radial functions $g_{jlM}(r,t)$ and $f_{jlM}(r,t)$ in Eq. (7), describing propagation of the TDDE in time. This system was solved using the matrix iteration method (MIM) [23].

The spin-resolved photoelectron momentum distribution (PMD) is calculated by projecting the Dirac bispinor $\Psi(\boldsymbol{r},T)$ at the end of the pulse on the set of the ingoing relativistic scattering states $\Psi^{-}_{\mu,\boldsymbol{p}}(\boldsymbol{r})$ [24]. These states describe the ionized electron with a given polarization, i.e. the spin direction in the electron's rest frame μ, and the asymptotic electron momentum $\boldsymbol{p}$.

In the non-relativistic limit, the TDDE with the vector potential described by Eq. (5) and Eq. (6) corresponds to the commonly used attoclock setup [12, 25]. In this setup, the target atom described by the SAE potential $V(r)$ is interacting with a CP laser pulse with the base frequency ω and the peak field strength E_0. The presently employed TDDE approach differs from the non-relativistic picture in several aspects. The most important feature is the possibility of the description of relativistic spin-related effects, in particular the SF effect, which is the main goal of the present work. We retain the coordinate dependence of the vector potential in our calculations. This way we account for non-dipole effects in the laser-atom interaction, which lead to the break-down in the conservation of canonical momentum [12, 26]. For the presently considered pulse intensities of the order of 10^{14} W/cm^2, non-dipole effects are not important. However, we retain these effects in our calculations for the sake of completeness and because it is not always easy to disentangle various relativistic effects in the Dirac framework. Meanwhile, such effects can be easily separated in the simplified semi-relativistic treatment based on the Breit-Pauli Hamiltonian. This offers a convenient means to study the contributions of various relativistic effects. We will use this possibility to interpret the results of the TDDE calculations. We will present below some results of the calculations using the Breit-Pauli approach. The theoretical framework of this approach is described in the next section.

B. Breit-Pauli framework

The semi-relativistic Breit-Pauli approach takes into account the relativistic effects up to the order of $1/c^2$ [27]. Breit-Pauli Hamiltonian has been recently used to investigate spin-orbit effects in strong field ionization with linearly polarized light [28]. The Breit-Pauli formulation is based on a systematic expansion of the TDDE in powers of $1/c$ [24]. Such an expansion leads to the following Hamiltonian describing the atom-laser field system:

$$\hat{H} = \frac{(\hat{\boldsymbol{p}} + \boldsymbol{A}(t))^2}{2} + V(r) + \hat{V}_{so} + \hat{V}_{smf} \ , \tag{8}$$

where

$$\hat{V}_{so} = \frac{1}{2c^2 r}\frac{dV(r)}{dr}\hat{\boldsymbol{l}} \cdot \hat{\boldsymbol{s}} \tag{9}$$

is the SO interaction, and

$$\hat{V}_{smf} = \frac{1}{c}\boldsymbol{H} \cdot \hat{\boldsymbol{s}} \tag{10}$$

is an operator describing interaction of electron spin and magnetic field of the pulse. The vector potential in Eq. (8) is a non-relativistic limit of the relativistic definition given by Eq. (5) and Eq. (6), which we obtain taking the limit $c \to \infty$.

The Hamiltonian (8) acts in the Hilbert space of the two-component spinor wavefunctions, which we represent as

$$\Psi(\boldsymbol{r}, t) = \sum_{l,m,\mu}^{l_{\max}} f_{lm\mu}(\boldsymbol{r}, t) Y_{lm}(\boldsymbol{r}) v_\mu \ . \tag{11}$$

Here v_μ are two-component spinors, $Y_{lm}(\boldsymbol{r})$ is the spherical function, and $f_{lm\mu}(r)$ are found by solving the time dependent Schrödinger equation for the wavefunction (11) with the Hamiltonian (8). The computational details are rather similar to those used to solve the TDDE, and we will not dwell on them.

We retain in the expression for the Breit Hamiltonian (8) only relativistic corrections involving the electron spin. The complete Breit Hamiltonian contains a number of other terms of the order of $1/c^2$, such as the kinematic term taking into account corrections due to the relativistic kinematics, and the Darwin term [27]. We omit these terms in the calculations in the Breit-Pauli framework which we present below. Our goal in performing these calculations was merely illustrative. By switching on and off the interactions (9) and (10) containing the electron spin, we can gauge their role in the SF process.

In the essentially non-relativistic regime with the field parameters under consideration, the Breit-Pauli results are typically very close to those in the TDDE approach. One could, in principle, adopt an entirely perturbative treatment, based on the complete Breit-Pauli Hamiltonian which takes into account relativistic effects up to the order of $1/c^2$ and adding relativistic corrections describing the leading non-dipole effects in the atom-field interaction, as we did in [29]. Such a calculation would be, however, technically more challenging and less transparent conceptually. As one can see from Eq. (9) the SO interaction operator behaves as r^{-3} for small r for the systems with the Coulomb core. This operator is, therefore, not self-adjoint unless we take a proper care of the domain of its definition. For instance we can require it to act only on the wave functions vanishing at the origin, so that its matrix elements converge. We coped with this problem in the present calculation using the Breit-Pauli framework by introducing a regularization for the SO interaction operator (9), making its singular behavior at $r = 0$ less severe. This, however, introduces an additional regularization parameter in the calculation, which makes the whole procedure not an entirely *ab initio* one. The Dirac framework, on the other hand, is, of course, a completely *ab initio* approach.

III. RESULTS AND DISCUSSION.

We will concentrate below on the np orbitals of various target atoms. With this choice we will clearly see the difference between the patterns of the angular attosecond streaking of the electrons which underwent the spin reversal (SF) and those which did not. We shall demonstrate that this difference comes in a large part from the SO interactions during the initial stage of the evolution of the atom in the external field. At this stage, the electron is close to the atomic core and the SO interaction (9), which falls fast with the distance, is the strongest. For an ns-state, the expectation value of the SO interaction operator (9) is zero. Thus we concentrate the initial states of the p symmetry. Furthermore, if we wish to track the electron spin direction, it is better to analyze the evolution from the states with a definite electron spin in the initial state. This dictates our choice of the initial states of the p symmetry with the total momentum $j = 3/2$ and its projection on the z-axis $m_j = 3/2$. Clearly, in such a state the electron spin is aligned along the $z-$ axis, and has a projection $m_s = 1/2$ on this axis.

We start presentation of our results with the atomic hydrogen in the $2p_{3/2}$ initial state. Figs. 1 and 2 display, respectively, the PMD $P(p_y, p_z)$ in the polarization (y, z) plane and the radially integrated PMD:

$$P(\phi) = \int P(p_y, p_z) dp \ . \tag{12}$$

Here $p = \sqrt{p_y^2 + p_z^2}$ with $p_y = p\cos\phi$ and $p_z = p\sin\phi$ in the presently employed polar coordinates. In Figure 2, as well as further in Figure 4, Figure 6, and Figure 8 below, we scale the PMD for the SF ionization to be able to show both distributions on the same plot.

By inspecting the PMD presented in Figure 1, we observe that ionization accompanied by the SF process leads to an additional main lobe rotation as compared to ionization without spin reversal. In the attoclock experiments, such an additional angular rotation would be interpreted as a delay of the SF ionization relative to the ionization without the spin reversal.

This behavior seems to be a general feature of the spin flip tunneling ionization, as can be surmised from the results shown in Figure 1-Figure 6, for ionization of hydrogen (Figure 1,Figure 2), hydrogen-like ion with nuclear charge $Z = 2$ (Figure 3,Figure 4), and boron and gallium (Figure 5,Figure 6) targets. The relative time delays can be estimated as $\tau = \theta/\omega$, where θ is the angle of the additional main lobe rotation of the SF PMD as compared to the PMD of ionization without spin reversal. From the data shown in Figure 1-Figure 6 we obtain the time delays of 126 as and 192 as (hydgrogen for the field strengths $E_0 = 0.0534$ a.u., and $E_0 = 0.04$ as, respectively), 422 as (hydrogen-like ion with $Z = 2$), 214 as (boron), and 318 as (gallium).

a) Without spin flip, $E_0 = 0.0534$ a.u. **b)** With spin flip, $E_0 = 0.0534$ a.u.

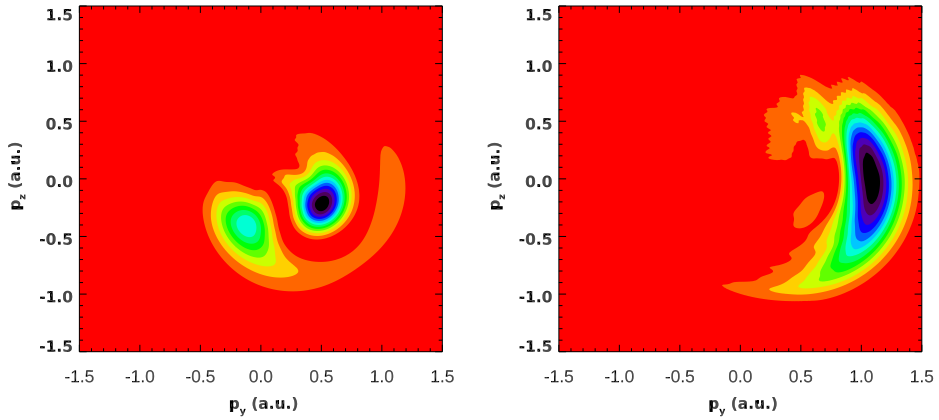

c) Without spin flip, $E_0 = 0.04$ a.u. **d)** With spin flip, $E_0 = 0.04$ a.u.

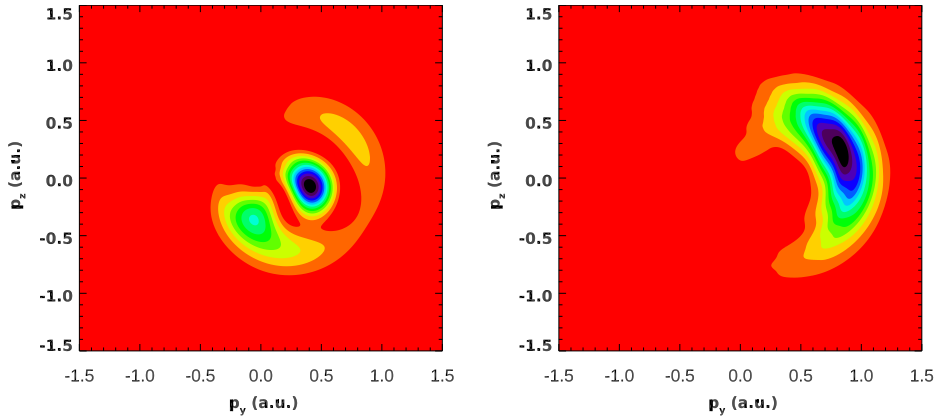

FIG. 1: PMD of hydrogen in the polarization plane, the $2p_{3/2}$ initial state with $\omega = 0.057$ a.u.

a) $E_0 = 0.0534$ a.u. **b)** $E_0 = 0.04$ a.u.

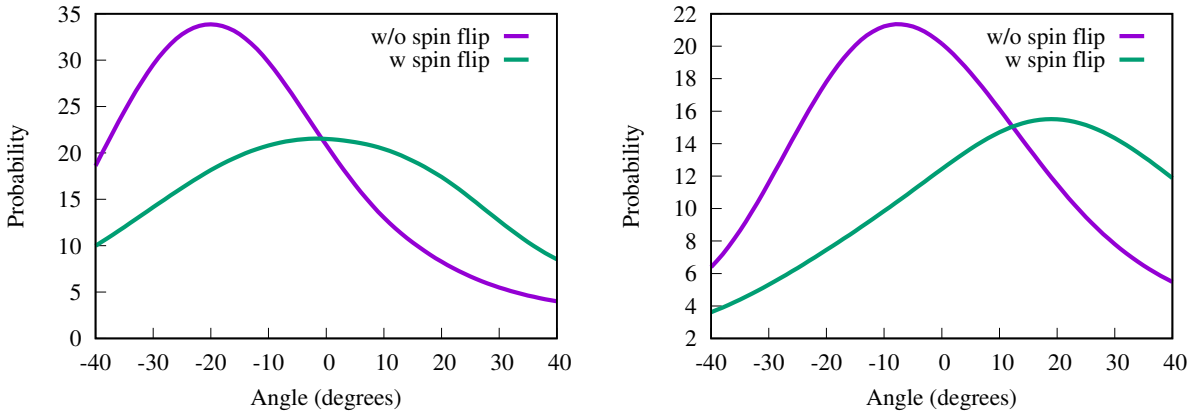

FIG. 2: Radially integrated PMD in the polarization plane, hydrogen in the $2p_{3/2}$ initial state, $\omega = 0.057$ a.u.

To elucidate the reason for such a behavior we perform addition calculations using the Dirac and the Breit-Pauli (BP) frameworks for a model screened hydrogen atom described by the potential:

$$V(r) = -\frac{1+3e^{-r}}{r} \tag{13}$$

with the energy of the $2p_{3/2}$ initial state $E = -0.351274$ a.u. In doing so, we employ the BP Hamiltonian (8) which includes the relativistic corrections responsible for the electron spin dynamics. The terms in the Hamiltonian corresponding to these corrections can be switched on and off, providing a convenient means of gauging their relative importance.

Figure 7a and Figure 7b show the PMD's obtained using the Dirac framework for the ionization with and without the spin reversal. As in the previous examples, we see the PMD for the SF ionization that is rotated with respect to the ionization without the spin reversal. The plot of the radially integrated PMD shown in Figure 8, derived from Figure 7a and Figure 7b, allows to estimate this rotation angle as $\theta \approx 72$ degrees, which can be interpreted as a relative time delay $\tau = \theta/\omega \approx 533$ as.

Figure 7c and Figure 7d show results of the calculations using the BP framework, with the SO interaction (Figure 7c) and the spin-magnetic field interaction (Figure 7d) switched off, respectively. We performed the BP calculation for the initial $2p$ state of the potential (13) with $m_l = 1$ and $\mu = 1/2$, which is a non-relativistic counterpart of the relativistic $2p$ state with $j = 3/2$ and $m_j = 3/2$ that we used in the TDDE calculations. One can observe that, upon switching off the SO interaction, the PMD for the SF ionization as rendered by the BP calculation is virtually indistinguishable from the PMD for the ionization without the SDF as given by the TDDE calculation.

This observation is yet more clearly illustrated in Figure 8 where we display the radially integrated angular distributions for the TDDE and various versions of the BP calculations. We notice that the results of the TDDE calculation for the ionization without the spin reversal are very close to those of the BP calculation with the SF and SO interaction (9) set to zero. In this version of the BP calculation, only the spin-magnetic field interaction is taken into account. These results clearly suggest the following scenario of SF ionization in the case when the SO interaction is absent. All the ionized electrons are born in the spin up state, coinciding with the spin orientation of the initial state of the target. The reversal of the spin direction in this scenario may occur only during the subsequent evolution of the system under the influence of the magnetic field of the pulse. In this scenario, therefore,

there is no tunneling time delay of the SF ionization with respect to the ionization without spin reversal.

Conversely, if we switch off the interaction of the electron spin with the pulse magnetic field (results marked as $H = 0$ in Figure 8) we see virtually no difference in the SF angular distribution comparing to the case of the BP calculation when both the SO and spin-magnetic field interactions are retained in the Hamiltonian (8).

Thus we can conclude that the SO interaction (9) is the main actor which is responsible for the observed effect of the delay of the SF ionization relative to the ionization without the spin reversal.

To elucidate the particular mechanism of the SO effect, we note that the SO interaction operator (9) falls fast with the distance from the origin. Its action, therefore, is limited to the immediate vicinity of the atom, and only states localized in this vicinity might participate in producing the observed effects of SF ionization.

In Figure 9 we show the decomposition of the BP final state wave-function. The Figure shows the norms $N_{lm\mu} = ||f_{lm\mu}||$ of the coefficients in expansion (11) for various l, m, μ. We show only the largest contributions for the spin up and spin down components of the wave function. We also show contributions of the bound $2s\mu$ and $2p\mu$ states to these norms. As one can see, in all the cases shown in Figure 9, the bound $2s$ and $2p$ states contributions by far dominate the norms $N_{lm\mu}$ for both the spin up and spin down states.

This observation suggests the following scenario of the spin down states production. The initial $2p$ state with $m = 1$ and $\mu = 1/2$ is coupled to the other spin up states $2lm$ by the electric field of the pulse, which produces Rabi-like oscillations, populating all the $2lm\mu$ states with $\mu = 1/2$. Next, the SO interaction comes on the stage. In the coupling scheme $lm\mu$ that we use matrix, the elements $\langle lm\mu|V_{so}|l'm'\mu'\rangle$ of the SO interaction (9) are non zero only when $l = l'$ and $m + \mu = m' + \mu'$ [27]. The SO interaction, therefore, couples $2p0\frac{1}{2}$ and $2p1 - \frac{1}{2}$ states producing the spin down states. The spin down $2p1 - \frac{1}{2}$ state, in its turn, is coupled by the electric field of the pulse to the $2lm$ spin down states. Then, the Rabi-like oscillations induced by the field populate the manifold of the spin down $2lm$ states.

The $2pl - \frac{1}{2}$ states undergo further the 'normal' spin-conserving non-relativistic tunneling ionization producing the spin down ionized electrons. As we see from Figure 9, the two main actors might be the spin down $2p0$ and $2p1$ states which have comparable populations.

To illustrate the plausibility of this scenario we show in Figure 10 results which we obtain

within the following simplified model. In the discussed scenario, the spin down ionization can be roughly pictured as tunneling ionization from a superposition of the states with energy separation approximately equal to the frequency of the Rabi-like oscillations. For the employed field strength $E_0 = 0.0534$a.u. and the $n = 2$ states we can estimate this frequency as $\Omega \approx 0.1$ a.u. In Figure 10 we show results obtained if we use the strong field approximation (SFA) [30, 31] to compute the PMD for the ionization from a superposition of the two states separated by the energy interval $\Delta = 0$ (Figure 10a) and $\Delta = 0.1$ a.u. (Figure 10b). One can see that we indeed obtain the rotated PMD in the second case in agreement with the results of the TDDE calculations we discussed above.

a) Without spin flip, $E_0 = 0.0534$ a.u. **b)** With spin flip, $E_0 = 0.0534$ a.u.

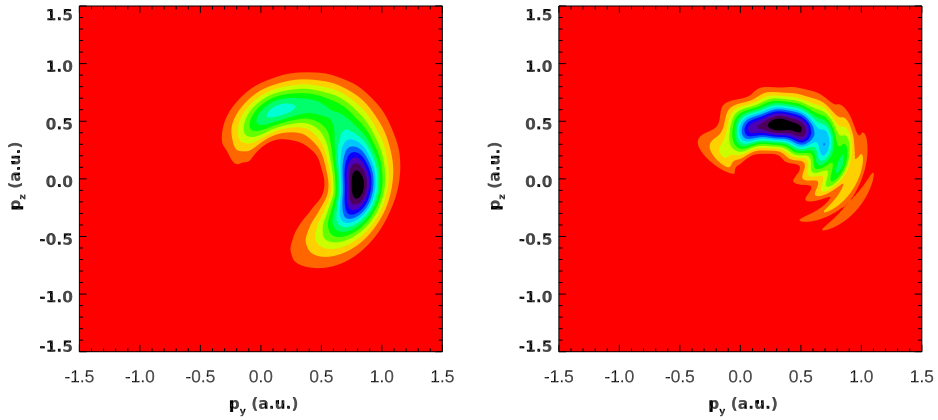

FIG. 3: PMD in the polarization plane, $\omega = 0.057$ a.u., hydrogen, $Z = 2$, $2p_{3/2}$ initial state

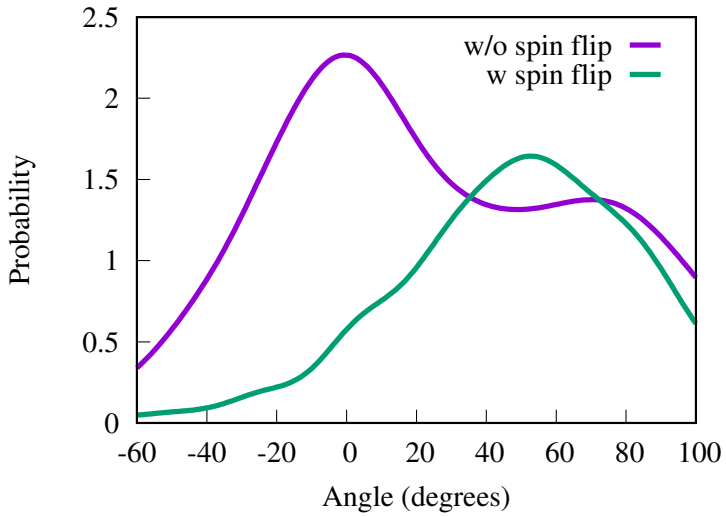

FIG. 4: Momentum integrated PMD in the polarization plane, $\omega = 0.057$ a.u., hydrogen, $Z = 2$, $2p_{3/2}$ initial state

a) Without spin flip, $E_0 = 0.03$ a.u., B **b)** With spin flip, $E_0 = 0.03$ a.u., B

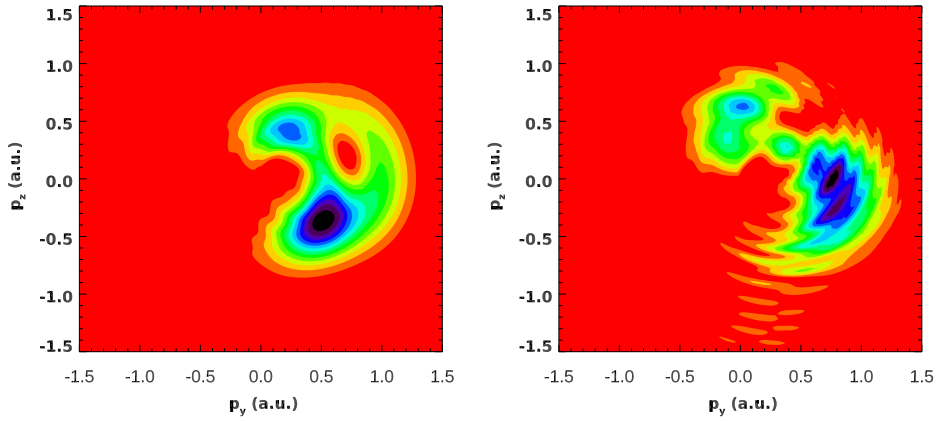

c) Without spin flip, $E_0 = 0.04$ a.u., Ga **d)** With spin flip, $E_0 = 0.04$ a.u., Ga

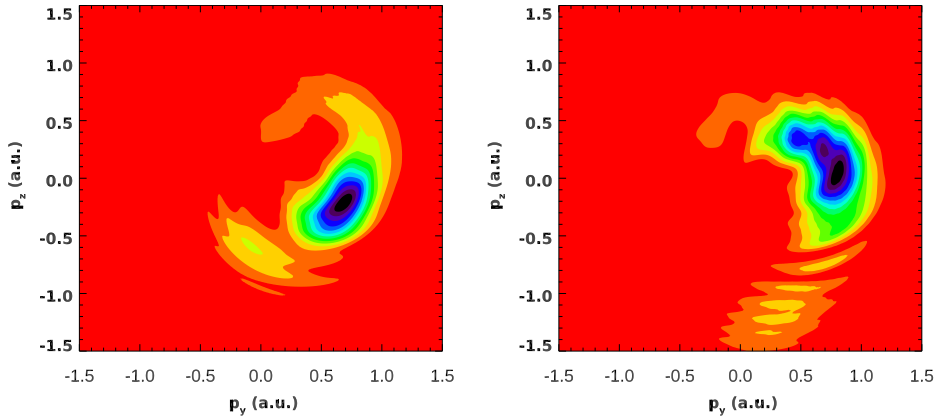

FIG. 5: PMD in the polarization plane, $\omega = 0.057$ a.u., Boron and Gallium targets, $2p_{3/2}$ initial state

a) $E_0 = 0.0534$ a.u., B **b)** $E_0 = 0.0534$ a.u., Ga

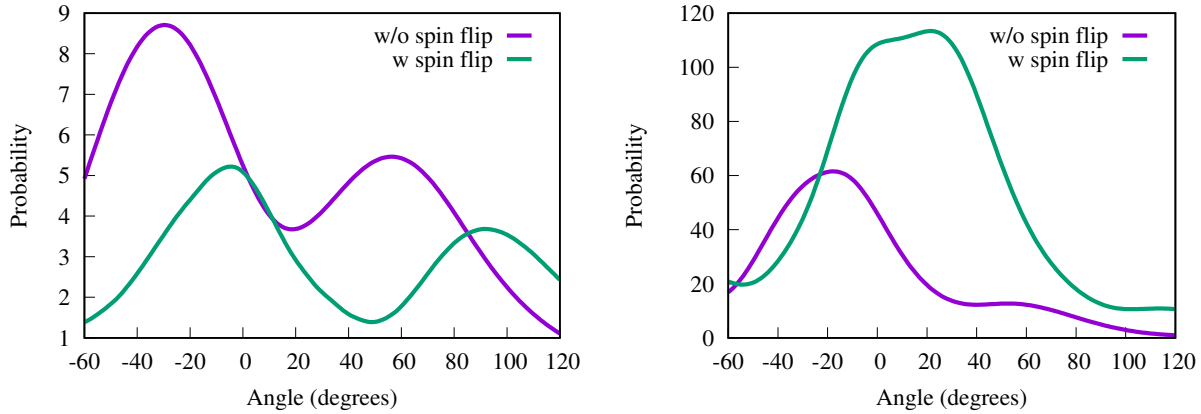

FIG. 6: Momentum integrated PMD in the polarization plane, $\omega = 0.057$ a.u., Boron and Gallium, $2p_{3/2}$ initial state

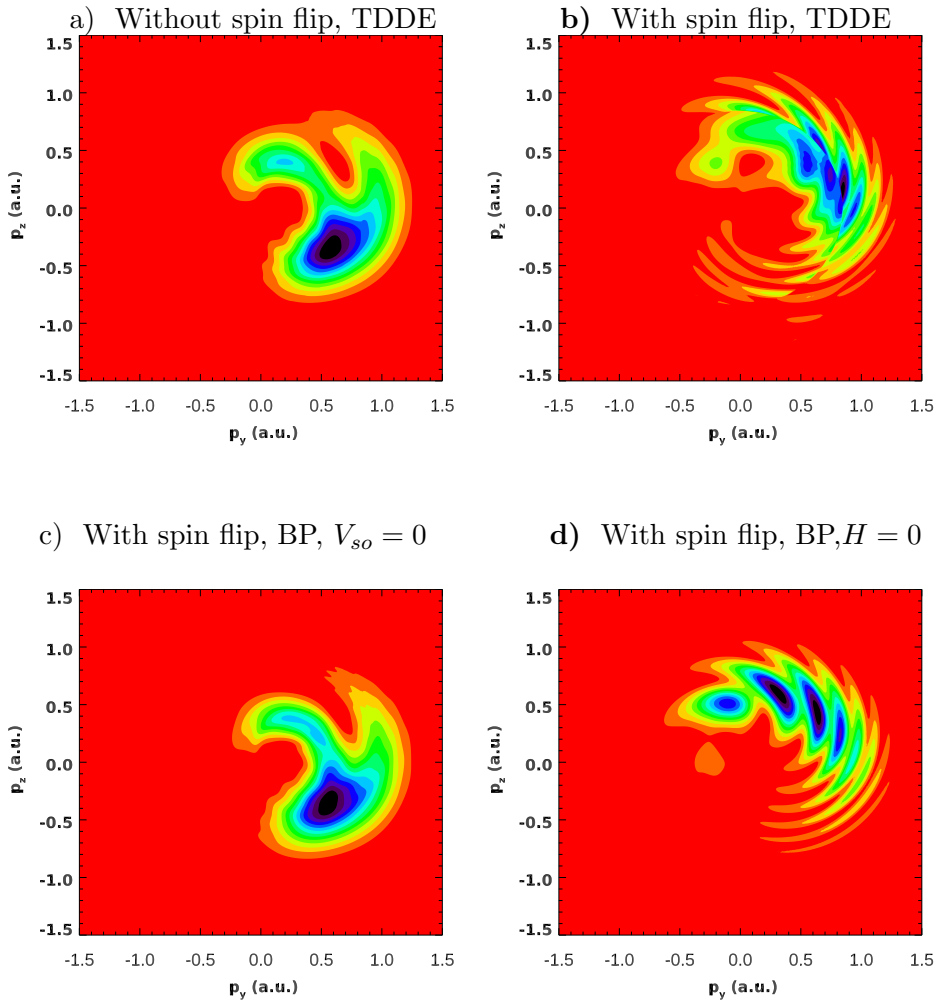

FIG. 7: PMD in the polarization plane, $\omega = 0.057$ a.u., $E_0 = 0.0534$ a.u., screened hydrogen, TDDE and BP calculations, $2p_{3/2}$ initial state

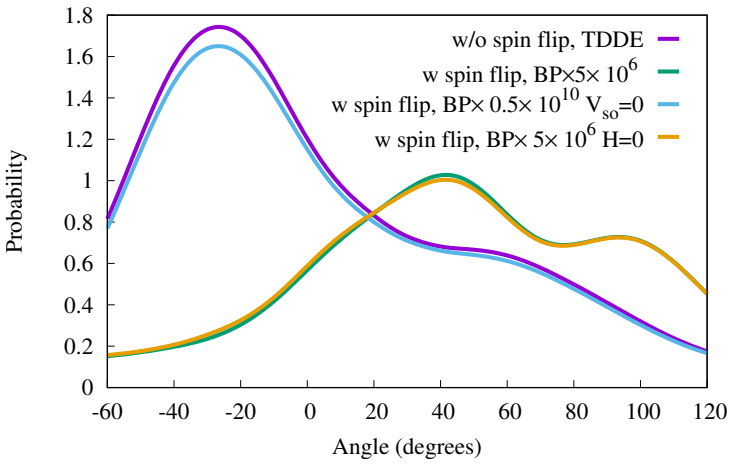

FIG. 8: Momentum integrated PMD in the polarization plane, $\omega = 0.057$ a.u., TDDE and BP calculations, screened hydrogen, $2p_{3/2}$ initial state

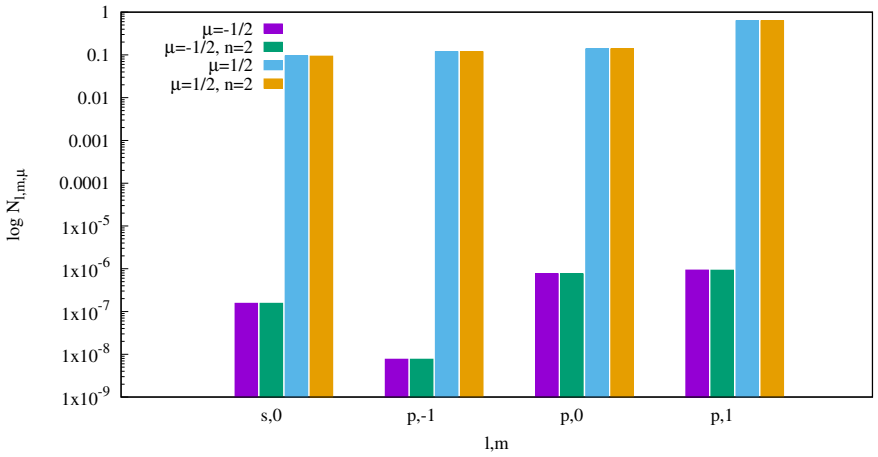

FIG. 9: Composition of the final state wave-function.

a) $\Delta = 0$ **b)** $\Delta = 0.1$

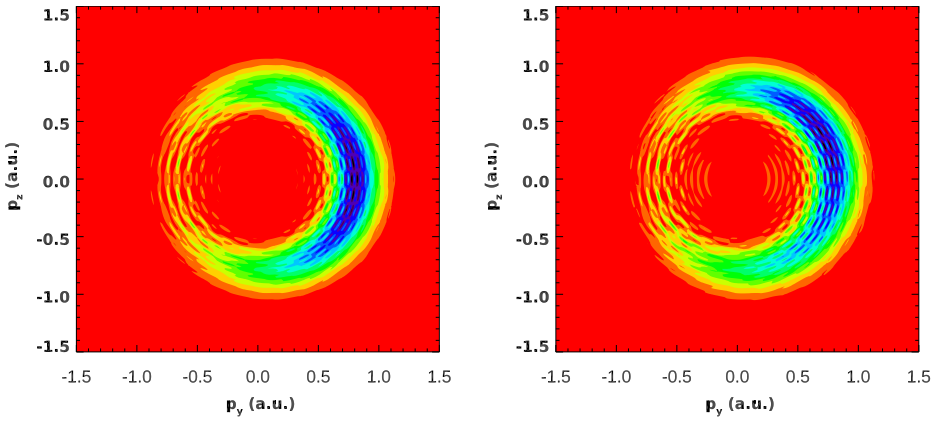

FIG. 10: PMD in the polarization plane, SFA for various energy splittings Δ.

IV. CONCLUSION

In this work we study systematically the effect of the spin reversal (spin-flip) on the process of tunneling ionization in the attoclock setting. We consider the hydrogen and heavier atoms in their initial np states driven by short circularly polarized laser pulses. As the marker of the SF effect, we study the photoelectron momentum distribution (PMD) in the plane of the laser polarization. We also consider the radially integrated PMD which allows to determine its angular offset relative to the electric field direction at the instant of tunneling. In the spirit of attoclock, we can relate this angular offset with the tunneling time delay $\tau = \theta/\omega$, after accounting the the long-range Coulomb interaction following ionization. The SF process generally increase this delay relative to the ionization process free from the spin reversal. We attribute the SF effect wholly to the SO interaction whereas the interaction of the photoelectron spin with the magnetic field of the driving field has virtually no SF effect.

The question of a non-zero tunneling time is hotly debated at the moment [12–15]. Simulation and measurement of this process on atomic hydrogen returns an essentially zero or negative tunneling time, within experimental and numerical accuracy [32, 33]. On the other hand, an experiment measuring tunneling time of Rb atoms through an optical barrier reported 0.61 milliseconds for the lowest energy at which tunneling was observed [35]. At the heart of the attoclock tunneling time debate is the question of absolute time (or time zero) when tunneling begins, which is assumed to be at the peak of the laser field. Here, we bypass this question by comparing the relative delay between the electrons which experience a spin flip and those that do not. This is similar to the linear streaking approach, which always extracts a relative (rather than the absolute delay) by comparing streaking traces from two different ionization events.

In the context of the attoclock measurements of strong field ionization, our modelling indicates that the SF process results in an increased angular offset. This angular offset seems to be due to the time-delay associated with the spin flip prior to tunneling. Spin-resolved attoclock experiments can therefore be used to investigate spin-flip dynamics during the strong field ionization process. Such experiments can take advantage of the fact that strong field ionization with circularly polarized light produces spin polarization by predominantly selecting counter-rotating electrons [34]. Using momentum gating to filter out corotating

electrons, it should be possible to isolate SF electrons in the angular-resolved photoelectron measurements obtained by the attoclock.

Recent experiments highlight the role of electron SF in photoionization of atoms [4] and molecules [9] using Reconstruction Attosecond Beating by Interference of Two-photon Transitions (RABBIT) measurements. However, SF dynamics have not been experimentally observed in strong field ionization. Our work suggests that a signature of SF during the tunnel ionization of atoms may be observable using the attoclock set-up. Extending this to molecules is more challenging due to the dependence of the attoclock interpretation on the initial state, which is harder to accurately describe in molecules compared to atoms [36, 37].

Another notable observation is that the SF effect is related to the Rabi-like oscillations. Our simulations return the PMD at the end of the photoelectron propagation to the detector. It would be tempting to trace this propagation and to resolve the Rabi oscillations in real time.

V. ACKNOWLEDGMENTS

This work was supported by the Discovery Grant DP230101253 from the Australian Research Council. A.S.L. acknowledges NSF Investigator-Initiated Research Grant, "Strong Field Physics with a Twist", Award No. 2208040. Resources of the National Computational Infrastructure facility have been utilized.

[1] H. R. Reiss and D. P. Crawford, *Relativistic photoionization*, in *ICONO '98: Ultrafast Phenomena and Interaction of Superstrong Laser Fields with Matter: Nonlinear Optics and High-Field Physics*, edited by M. V. Fedorov, V. M. Gordienko, V. V. Shuvalov, and V. D. Taranukhin, International Society for Optics and Photonics (SPIE, 1999), vol. 3735, pp. 148 – 157.

[2] H. Wang, S. I. Bokarev, S. G. Aziz, and O. K. and, *Density matrix-based time-dependent configuration interaction approach to ultrafast spin-flip dynamics*, Molecular Physics **115**(15-16), 1898 (2017).

[3] H. Wang, T. Möhle, O. Kühn, and S. I. Bokarev, *Ultrafast dissipative spin-state dynamics triggered by x-ray pulse trains*, Phys. Rev. A **98**, 013408 (2018).

[4] S. Zhong, J. Vinbladh, D. Busto, R. J. Squibb, M. Isinger, L. Neoricić, H. Laurell, R. Weissenbilder, C. L. Arnold, R. Feifel, et al., *Attosecond electron-spin dynamics in Xe 4d photoionization*, Nature Communications **11**, 5042 (2020).

[5] I. Jordan, M. Huppert, S. Pabst, A. S. Kheifets, D. Baykusheva, and H. J. Wörner, *Spin-orbit delays in photoemission*, Phys. Rev. A **95**, 013404 (2017).

[6] M. Turconi, L. Barreau, D. Busto, M. Isinger, C. Alexandridi, A. Harth, R. J. Squibb, D. Kroon, C. L. Arnold, R. Feifel, et al., *Spin-orbit-resolved spectral phase measurements around a fano resonance*, J. Phys. B **53**(18), 184003 (2020).

[7] R. Khademhosseini, P. C. Deshmukh, and S. T. Manson, *Attosecond time delay in atomic photoionization: Angular-dependent transition from dipole to quadrupole and spin-flip dynamics*, Phys. Rev. A **108**, 063107 (2023).

[8] M. A. Alarcón, A. Plunkett, J. K. Wood, D. Biswas, C. H. Greene, and A. Sandhu, *Quantum beats in two-color photoionization to the spin-orbit split continuum of ar*, Phys. Rev. A **108**, 033107 (2023).

[9] B. Grafstrom, A. Wang-Holtzen, J. Wang, P. H. Bucksbaum, J. P. Cryan, and A. S. Landsman, *Relativistic effects in molecular photoemission delays*, Phys. Rev. A **110**, L061101 (2024).

[10] P. Eckle, M. Smolarski, P. Schlup, J. Biegert, A. Staudte, M. Schöffler, H. G. Muller, R. Dörner, and U. Keller, *Attosecond angular streaking*, Nature Physics **4**(7), 565 (2008).

[11] P. Eckle, A. N. Pfeiffer, C. Cirelli, A. Staudte, R. Dorner, H. G. Muller, M. Buttiker, and

U. Keller, *Attosecond ionization and tunneling delay time measurements in helium*, Science **322**(5907), 1525 (2008).

[12] C. Hofmann, A. S. Landsman, and U. Keller, *Attoclock revisited on electron tunnelling time*, J. of Modern Optics **66**(10), 1052 (2019).

[13] A. S. Kheifets, *The attoclock and the tunneling time debate*, J. Phys. B **53**(7), 072001 (2020).

[14] U. S. Sainadh, R. T. Sang, and I. V. Litvinyuk, *Attoclock and the quest for tunnelling time in strong-field physics*, J. Phys. B **2**(4), 042002 (2020).

[15] C. Hofmann, A. Bray, W. Koch, H. Ni, and N. I. Shvetsov-Shilovski, *Quantum battles in attoscience: tunnelling*, Europ. Phys. J. D **75**, 208 (2021).

[16] M. Han, P. Ge, Y. Fang, X. Yu, Z. Guo, X. Ma, Y. Deng, Q. Gong, and Y. Liu, *Unifying tunneling pictures of strong-field ionization with an improved attoclock*, Phys. Rev. Lett. **123**, 073201 (2019).

[17] S. Eckart, *Holographic angular streaking of electrons and the Wigner time delay*, Phys. Rev. Research **2**, 033248 (2020).

[18] T. Driver, M. Mountney, J. Wang, L. Ortmann, A. Al-Haddad, N. Berrah, C. Bostedt, E. Champenois, L. DiMauro, J. Duris, et al., *Attosecond delays in X-ray molecular ionization*, Nature **632**, 762 (2024).

[19] R. Gutzler, M. Garg, C. R. Ast, K. Kuhnke, and K. Kern, *Light-matter interaction at atomic scales*, Nature Reviews Physics **3**, 441 (2021).

[20] I.A.Ivanov, *Relativistic calculation of the electron-momentum shift in tunneling ionization*, Phys. Rev. A **91**, 043410 (2015).

[21] I. A. Ivanov, *Spin-flip processes and nondipole effects in above-threshold ionization of hydrogen in ultrastrong laser fields*, Phys. Rev. A **96**, 013419 (2017).

[22] A. Sarsa, F. J. Gálvez, and E. Buendia, At. Data Nucl. Data Tables **88**(1), 163 (2004).

[23] M. Nurhuda and F. H. M. Faisal, *Numerical solution of time-dependent schrödinger equation for multiphoton processes: A matrix iterative method*, Phys. Rev. A **60**(4), 3125 (1999).

[24] A. Akhiezer and V. Berestetskii, *Quantum Electrodynamics* (John Wiley & Sons, 1965).

[25] I. A. Ivanov and A. S. Kheifets, *Time delay in atomic photoionization with circularly polarized light*, Phys. Rev. A **87**, 033407 (2013).

[26] A. S. Landsman, S. A. Cohen, and A. Glasser, *Onset and Saturation of Ion Heating by Odd-Parity Rotating Magnetic Field in a Field-Reversed Configuration*, Physical Review Letters

96(1), 015002 (2006).

[27] I. I. Sobelman, *Introduction to the Theory of Atomic Spectra* (Pergamon Press, New York, 1972).

[28] A. S. Maxwell, L. B. Madsen, *Relativisitc and spin-orbit dynamics at nonrelativistic intensities in strong-field ionization*, Physical Review A **110**, 033108 (2024).

[29] I.A.Ivanov, J. Dubau, and K. T. Kim, *Nondipole effects in strong-field ionization*, Phys. Rev. A **94**, 033405 (2016).

[30] V. S. Popov, *Tunnel and multiphoton ionization of atoms and ions in a strong laser field*, Physics-Uspekhi **47**, 855 (2004).

[31] S. V. Popruzhenko, *Keldysh theory of strong field ionization: history, applications, difficulties and perspectives*, Journal of Physics B: Atomic, Molecular and Optical Physics **47**(20), 204001 (2014).

[32] L. Torlina, F. Morales, J. Kaushal, I. Ivanov, A. Kheifets, A. Zielinski, A. Scrinzi, H. G. Muller, S. Sukiasyan, M. Ivanov, et al., *Interpreting attoclock measurements of tunnelling times*, Nat. Phys. **11**, 503 (2015).

[33] U. S. Sainadh, H. Xu, X. Wang, A. Atia-Tul-Noor, W. C. Wallace, N. Douguet, A. Bray, I. Ivanov, K. Bartschat, A. Kheifets, et al., *Attosecond angular streaking and tunnelling time in atomic hydrogen*, Nature **568**, 75 (2019).

[34] G. Armstrong, D. Clarke, J. Benda, J. Wragg, A. Brown, H. W. van der Hart, *Enhancing spin polarization using ultrafast angular streaking*, Physical Review A **103**, 053123 (2021).

[35] R. Ramos, D. Spierings, I. Racicot, A. M. Steinberg, *Measurement of the time spent by a tunnelling atom within the barrier region*, Nature **538**, 529 (2020).

[36] N. Suárez, A. Chacon, E. Pisanty, L. Ortmann, A. S. Landsman, A. Picón, J. Biegert, M. Lewenstein, M. Ciappina, *Above-threshold ionization in multicenter molecules: The role of the initial state*, Physical Review A **97**, 033415 (2018).

[37] L. Ortmann, A. AlShafey, A. Staudte, A. S. Landsman, *Tracking the Ionization Site in Neutral Molecules*, Physical Review Letters **127**, 213201 (2021).